Kurze Mitteilungen

Bis am 15. des Monats bei der Redaktion eingehende Kurze Mitteilungen werden in der Regel am 15. des folgenden Monats veröffentlicht. Es werden auch Manuskripte aus dem Ausland angenommen. Maximalumfang: 6 Schreibmaschinenseiten (alles inbegriffen)

Zwei isomere 4,7,12,15-Tetramethoxy-[2.2] paracyclophane*

Summary

The Hofmann-1,6-elimination reaction of 2,5-dimethoxy-4-methyl-benzyl-trimethylammonium hydroxyde led to a mixture of 2,5-dimethoxy-4-hydroxymethyl-toluene, di-(2,5-dimethoxy-4-methyl-benzyl)-ether and the two possible cyclic dimers of 2,5-dimethoxy-quinodimethane. The structure of these compounds was confirmed by NMR and mass spectra analyses.

Wir haben uns im Rahmen einer Untersuchung «intramolekularer Charge-Transfer-Komplexe» in der Cyclophanreihe auch mit der Synthese von [2.2] Paracyclophanen beschäftigt, in welchen der eine Benzolring (D) Elektronendonator- und der andere Benzolring (A) Elektronenakzeptoreigenschaften besitzt[1].

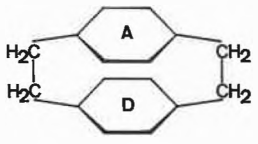

Substituenten:
in A: NO_2,CN,Keto-O
in D: CH_3,OH,$N(R)_2$

Eine kürzlich von REBAFKA und STAAB[2] publizierte Arbeit über ein «intramolekulares Chinhydron» veranlaßt uns, nachfolgend über die Synthese der zwei isomeren 4,7,12,15-Tetramethoxy-[2.2]paracyclophane 6a und 6b zu berichten. Die genannten Autoren haben sowohl bei der direkten Photolyse der beiden Tetramethoxy-dithia-[3.3]paracyclophane 1a und 1b in Triäthylphosphit als auch bei der Gasphasenpyrolyse der entsprechenden Disulfone nur das Isomere 6b mit gestaffelter Anordnung der Methoxygruppen erhalten.

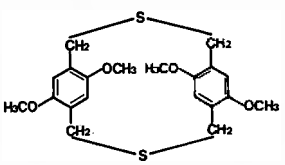

(1a)

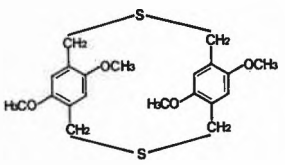

(1b)

* Eingegangen am 25. Februar 1974. Teilweise vorgetragen am 5. Internationalen Farbensymposium in Basel (24. bis 28. September 1973). Vgl. auch *Chimia 27* (1973) 641.

[1] Zur Problemstellung vgl. auch J.W. VERHOEVEN *et al.*, *Tetrahedron Letters 1973*, 1649. Zu dem Fall der «intramolekularen Chinhydrone» vgl. die Anmerkung am Schluß dieser Mitteilung.

[2] W. REBAFKA und H.A. STAAB, *Angew. Chem. 85* (1973) 831.

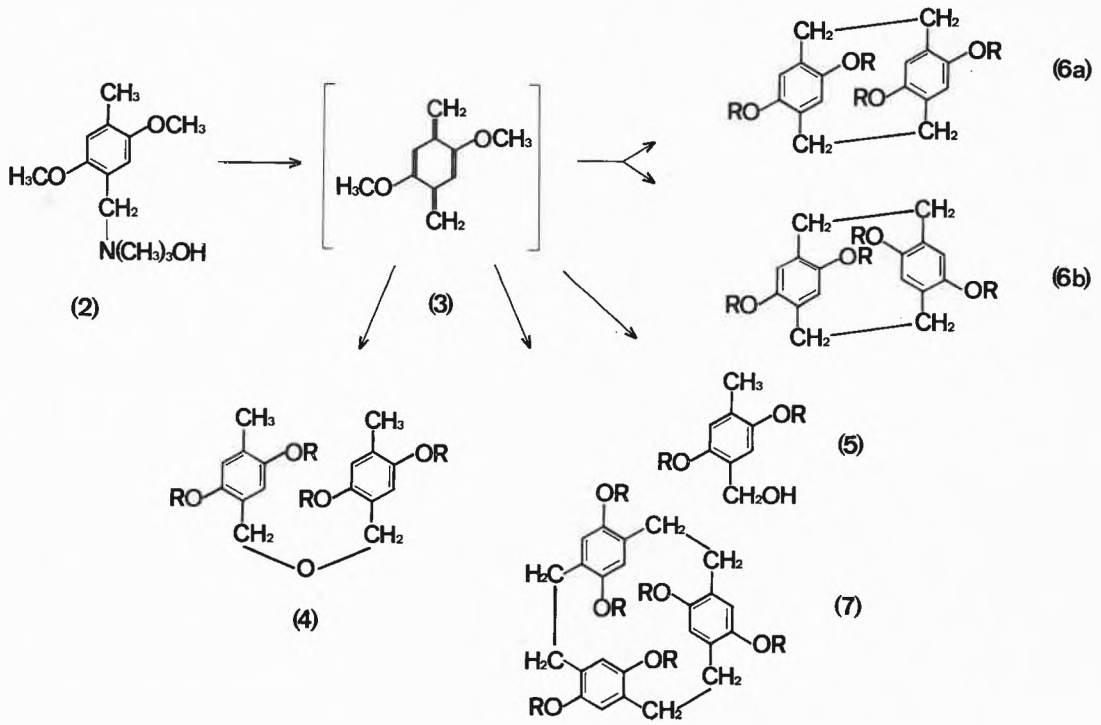

Wir haben gefunden, daß das Isomere mit pseudogeminaler Konfiguration (6a) durch Hofmann-1,6-Eliminierung mit 2,5-Dimethoxy-4-methyl-benzyl-trimethylammonium-hydroxyd (2) darstellbar ist. Diese Eliminierungsreaktion wurde schon von TAYLOR und KOLESINSKI[3] beschrieben. Die Autoren begnügten sich aber mit der Isolierung und Untersuchung der schwerlöslichen linearen Polymere.

Der toluollösliche Anteil (etwa 50%) aus der Eliminierungsreaktion wurde säulenchromatographisch (Alox II neutral, Hexan/Essigester 80/20) aufgetrennt. In den ersten Fraktionen konnte durch gekoppelte GC/MS die Anwesenheit der isomeren zyklischen Dimere 6a und 6b nachgewiesen werden. Die Ausbeuten der beiden Ringsysteme betragen 34% für 6b und 2 bis 3% für 6a. Diese Fraktionen enthalten noch zyklisches Trimeres 7 und den Dibenzyläther 4 (Ausbeute $< 1\%$). In den letzten Fraktionen der Säulenchromatographie liegt der Benzylalkohol 5 rein vor (Ausbeute etwa 1%, Smp. 76 bis 78°). Zur Gewinnung der reinen Verbindungen 6a und 6b müssen diese vom zyklischen Trimeren 7 und dem Dibenzyläther 4 getrennt werden. Dies gelingt gaschromatographisch (3% XE-60) und durch fraktionierte Kristallisation aus absolutem Äthanol.

Die beiden Tetramethoxy-[2.2]paracyclophane ergeben – auch in bezug auf die Intensität der Fragment-Ionen – praktisch identische Massenspektren. Ein merklicher Unterschied zeigt sich in den R_f-Werten auf Kieselgelplatten ($\Delta \sim 0{,}1$) und im Schmelzverhalten. Kristalle des Ringsystems 6a schmelzen – im Gegensatz zu 6b (Smp. 120 bis 121°) – erst bei etwa 230° (unkorr.)[4].

Einen weiteren, für die Strukturzuordnung wichtigen Unterschied zwischen 6a und 6b zeigt das ^{1}H-NMR-Spektrum (vgl. Tabelle 1). In den beiden isomeren Dithia-[3.3]paracyclophanen 1a und 1b findet man für die aromatisch gebundenen Protonen (H_a) die gleiche chemische Verschiebung (δ 6,61 ppm). Mit dem Übergang in die [2.2]Paracyclophan-Struktur ist erwartungsgemäß eine diamagnetische Verschiebung der H_a-Protonen verbunden. Der δ-Wert des Isomeren mit pseudo-

Tabelle 1. Chemische Verschiebung der Protonen in 1a, 1b, 6a, 6b und 4. Vergleich mit 2,5-Di-chlormethyl-hydrochinondimethyläther (8), 2,11-Dithia-[3.3]paracyclophan (9) und [2.2]-paracyclophan (10). Spektren aufgenommen in $CDCl_3$ mit TMS als internem Standard (100 MHz, δ in ppm)

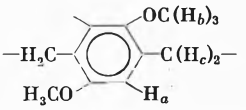

	H_a	H_b	H_c
8	6,88 (S)	3,81 (S)	4,58 (S)
1a[d]	6,61 (S)	3,74 (S)	4,07/3,92/3,52/3,37[e]
1b[d]	6,61 (S)	3,67 (S)	4,51/4,36/3,34/3,19[e]
9[f]	6,84 (S)	–	3,80 (S)
6a	5,88 (S)	3,64 (S)	3,57/3,48/2,64/2,56[e]
6b	6,10 (S)	3,66 (S)	3,20/3,12/2,69/2,61[e]
10[g]	6,37 (S)	–	3,03 (S)
4	6,71/6,98 (2S)	3,80/3,77 (2S)	4,62 (2,22 Aryl-CH_3)

d Versuchsweise Zuordnung (Smp. 1a: 215 bis 217°, 1b: 242 bis 246°; vgl. dazu auch REBAFKA und STAAB, *loc. cit.*[2]). *e* AA'BB'-Spektrum (angegeben sind die vier intensivsten Signale). *f* F. VÖGTLE, *Chemiker-Ztg. 94* (1970) 316. *g* Aufgenommen in $CDCl_3$ + DMSO

geminaler Konfiguration (6a) liegt bei 5,88 ppm, derjenige für die *pseudoortho*-Konfiguration (6b) bei 6,10 ppm. Eine verstärkte Abschirmung der H_a-Protonen wurde auch im analog aufgebauten 4,7,12,15-Tetramethyl-[2.2]paracyclophan (mit verdeckter Anordnung der Methylgruppen) gefunden[5]. Aus Tabelle 1 ist ersichtlich, daß sich die unterschiedliche Stellung der Methoxygruppen in den zwei Isomeren auch auf die chemische Verschiebung der aliphatisch gebundenen Brückenprotonen (H_c) auswirkt. Beim Isomeren 6a liegen A- und B-Teil des AA'BB'-Spektrums merklich weiter auseinander.

Anmerkung bei der Korrektur: REBAFKA und STAAB haben inzwischen auf photochemischem Wege auch das pseudogeminale Tetramethoxy[2.2]paracyclophan darstellen können. Aus dieser Verbindung wurde das intramolekulare Chinhydron mit pseudogeminaler Konfiguration synthetisiert (Vortrag vor der Deutschen Chemischen Gesellschaft in Freiburg im Breisgau am 14. Januar 1974 und Privatmitteilung).

Wir sind den Herren Dr. H. ABEGG, F. RASCHDORF (GC und GC/MS-Kopplung), Dr. H. FUHRER (NMR) und Dr. H. HÜRZELER (MS) aus der Zentralen Funktion Forschung der CIBA-GEIGY AG in Basel für instrumentalanalytische Untersuchungen zu großem Dank verpflichtet.

ALEXANDER DAVATZ und
WALTER JENNY*

Institut für organische Chemie der Universität Bern und CIBA-GEIGY AG, Basel,
Forschungslaboratorien der Division Farbstoffe und Chemikalien

* Anfragen sind zu richten an W. J., CIBA-GEIGY AG, Basel.

[3] L. D. TAYLOR and H. S. KOLESINSKI, *Polymer Letters 1* (1963) 117–9.

[4] Die beiden isomeren 4,7,12,15-Tetramethyl-[2.2]paracyclophane zeigen eine Schmelzpunktdifferenz ähnlicher Größenordnung (*pseudoortho*-Konfiguration: 105 bis 107°, pseudogeminale Konfiguration 230 bis 231°). Vgl. TETSUO OTSUBO *et al.*, *Tetrahedron Letters 1971* (Nr. 50) 4805.

[5] TETSUO OTSUBO *et al.*, *Tetrahedron Letters 1971* (Nr. 50) 4803.

An Electronically Integrating Actinometer for Quantum Yield Determinations of Photochemical Reactions *

Summary

An electronically integrating actinometer is described which is designed to provide routinely continuous reading under daylight conditions of the light flux absorbed in the photochemical sample solution and to exclude experimental errors due to manual handling in chemical actinometry. The detector system is based on the measuring of the flux difference in front and behind the sample cell using the absorption-fluorescence capacity of rhodamine B scintillator coupled with silicon semiconductor photoelements. The differential flux measurement is independent of incident wavelength and proportional to the light quanta absorbed, and it can be programmed to proceed until a preset number of light quanta is absorbed.

Introduction

Conventional determinations of photochemical quantum yields (Φ) are based on the measurement of the total light quanta absorbed in the sample solution as compared to a photochemical reference system of known quantum yield (chemical actinometer)[1]. The principal drawbacks of such measurements are that they are time consuming and that they must be done in the dark. This often results in relatively low precision.

In the following we describe an electronically integrating ("black box" instrument) actinometer designed to provide continuous recording of the light flux absorbed in the sample solution, and to exclude experimental errors due to manual handling. The system also includes the following features: (1) A compact and mechanically solid housing for the optical components, sample cell, etc., which fits neatly behind the exit of a light source in such a way that readings can also be taken under daylight conditions. (2) Provision for adequate measuring accuracy at relatively broad incident wavelength bandwidths (< 50 nm) as available from interference filter systems and monochromators. (3) Differential measurements of the light flux in front and behind the sample cell. (4) Flux measurement independent of incident wavelength. (5) Initial calibration of the integrator using conventional chemical actinometry. (6) Additional operating convenience such as automatic interruption of the photolysis at a preset number of light quanta absorbed.

Some of these features have been incorporated in other counters described in the literature. YIP and DICKINSON[2] constructed a simple digital integrator for the determination of the light flux. However, measurements were restricted to the direct use of a photomultiplier and to the light entering the sample cell. A similar approach was chosen by SCHULTZE and VOGEL[3] in which a photoresistor was substituted for a

* Received March 12, 1974.

[1] J. G. CALVERT and J. N. PITTS, Jr., *Photochemistry*, John Wiley & Sons, New York 1966, p. 587, 795.

[2] R. W. YIP and D. R. DICKINSON, *J. Sci. Instrum. 43* (1966) 758.

[3] H. SCHULTZE and H.-R. VOGEL, *Mol. Photochem. 5* (1973) 223.

photomultiplier. This modification appears to be even less satisfactory since the linearity of the integrator function cannot easily be obtained. BIRGE and JOHNSON[4] introduced a differentially measuring and wavelength-independent thermistor system at the expense of the integration function. Alternatively, the use of optical scintillators, which completely absorb light of a wide range of wavelengths and convert it with constant quantum efficiency to fluorescence emission, offers a more convenient way to operate an actinometer system at constant wavelength independent of the wavelengths used photochemically. YGUERABIDE[5] and MELHUISH[6] have shown that solutions of rhodamine B in ethylene glycol can serve as an adequate light-stable scintillator. The quantum efficiency of fluorescence proved to be completely independent of incident wavelength in the region 220–590 nm. Fluorescence of rhodamine B centers at 600 nm, in which region a variety of optoelectronic measuring elements are available. HEINZELMANN and LABHART[7] have used rhodamine B successfully in combination with electrical light measurements for actinometric purposes.

Instrumental Design

The design of our instrumentation is given in Figs. 1 to 3. Figs. 1 and 2 show the *detector unit (D)* composed of a thermostated *(T)* black anodized aluminium housing attached to the exit slit *(S_2)* of a monochromator *(Mo)*, and an electronically controlled shutter *(Sh)* behind which a beam splitter *(B)* (a polished thin quartz plate) reflects a portion of the radiation *(ca.* 4,9% at 300 nm[8]) onto a quartz cell C_1 (path length 4 mm) containing a 3 g/liter solution of rhodamine B in ethylene glycol[5]. The main beam continues through the sample quartz cell *(C_3*, path length 1 cm) to a closely fitted second scintillator cell *(C_2)* similar to C_1, which compensates for incomplete absorbance in C_3. A magnetic stirring motor *(SM)* is placed below C_3. The fluorescence photon fluxes are measured by silicon semiconductor photoelements, P_1 and P_2 (AEG BPY 71[9]), which are mounted at a distance of *ca.* 5 mm behind C_1 and C_2. These photoelements were chosen instead of photomultipliers in order to avoid the necessity for a highvoltage power supply. They exhibit a very satisfactory linear relationship between the incident quanta flux and the voltage produced (0 to 100 mV at 2 KΩ). Moreover, the dimension of the light-sensitive photoelement surface (9 × 20 mm) suffices to cover the entire lighted region of a conventional rectangular 1-cm uv cell. The edges of the cells are masked *(M)* in order to prevent incident flux being piped through the cell walls directly to the photoelements.

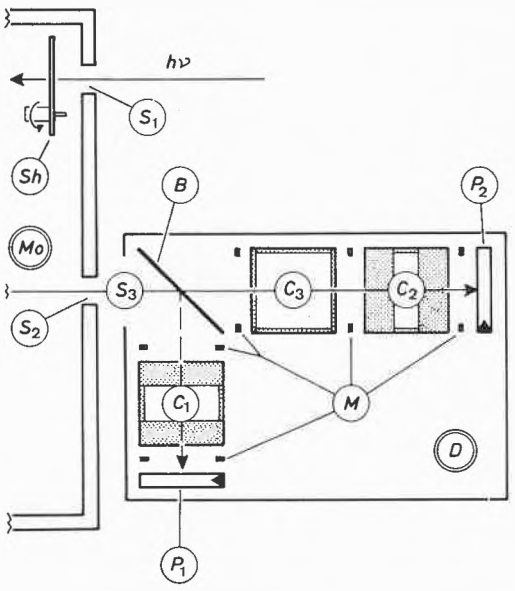

Fig. 1. Diagram of the detector unit *(D)*

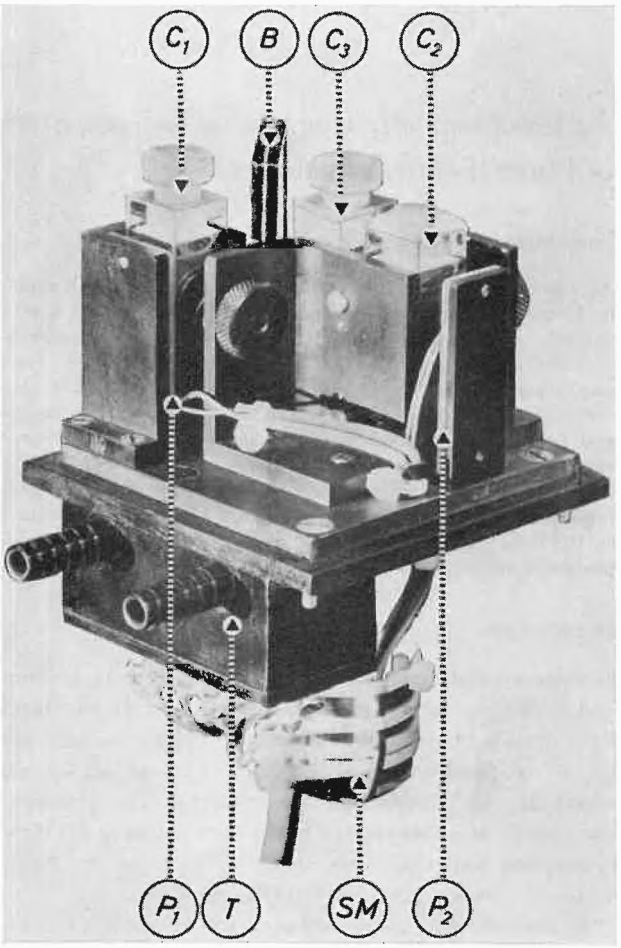

Fig. 2. View of the detector unit (without removable top)

B = Beam splitter, $C_{1,2}$ = scintillator cells, C_3 = sample cell, *M* = cell masks, *Mo* = monochromator, $P_{1,2}$ = photoelements, $S_{1,2}$ = entrance and exit slits of monochromator, S_3 = window of detector housing, *Sh* = mechanical shutter, *SM* = magnetic stirring motor, *T* = thermostated platform

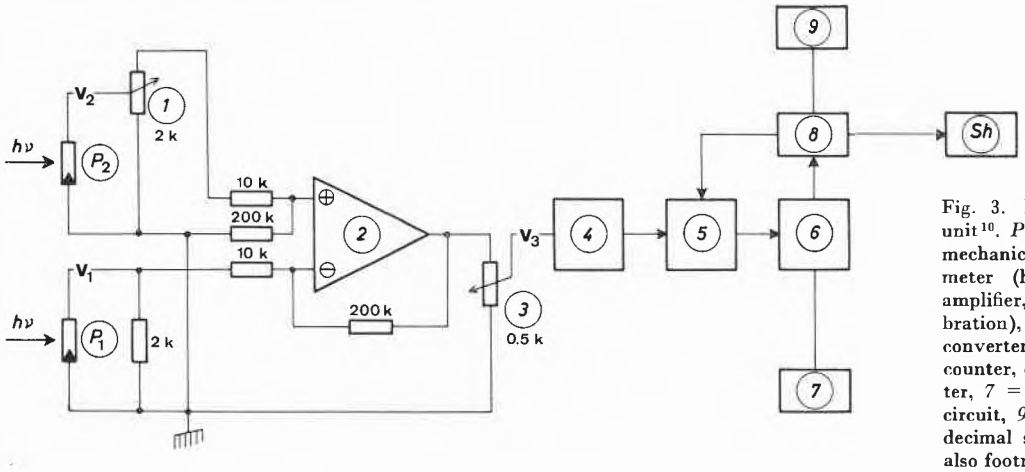

Fig. 3. Diagram of the integrator unit[10]. $P_{1,2}$ = Photoelements, *Sh* = mechanical shutter, *1* = potentiometer (balance), *2* = differential amplifier, *3* = potentiometer (calibration), *4* = voltage-to-frequency converter, *5* = decimal-place pre-counter, *6* = four-digit decimal counter, *7* = counter display, *8* = logic circuit, *9* = four-digit binary coded decimal switch (preset selector); see also footnote[11]

The diagram of the *integrator unit* is shown in Fig. 3. The parallel arrangement of the compensating photoelement P_2 and the 10-turn potentiometer *1* (Beckman Helipot 7246) provides for balancing of the differential amplifier *2* (gain 20) to 100 % light transmission in the sample cell *(C_3)*, and the second precision potentiometer *3* for the additional choice of a correction factor (calibration). Converter *4* operates with a minimum convertible voltage of 1 mV and exhibits linearity of the output frequency with input voltage in the range of 10 mV to 1 V within ±1 %. The temperature drift (−0,2 %/°C) of the four-layer diode (Motorola-1N5158) in *4* is eliminated by thermostatic control. The sawteeth pulses are received by a four-digit decimal counter *(6)*, with display *(7;* Omnicont Mo 5P), *via* a signal converter to TTL standards and an adjustable decimal-place pre-counter *(5)*. The displayed pulse sum is consequently[11] proportional to the number of light quanta absorbed in the sample cell *(C_3)* at any moment during the irradiation experiment, and it is independent of intensity fluctuations of the light source and changes in extinction of the sample solution. The logic circuit *8* interrupts as soon as the displayed pulse sum reaches a value which can be preset with a four-digit binary coded decimal switch *(9;* Omnicont CS 401-001), and it activates the mechanical shutter *Sh*.

Applicatory Extensions and Restrictions

Several complementary alterations to this actinometer system are possible without major changes in the basic units (detectors and integrators). *E.g.*, uv spectrometric product analysis in the present version requires transfer of the sample cell *(C_3)* into a spectrophotometer. Appropriate slits in the cell holder of C_3 and the removable top of the detector housing could allow for simultaneous spectrophotometric monitoring of the sample solution with irradiation, using the cross beam principle *(cf.*[3]*)*. In a simpler version, albeit limited to monitoring the optical density changes of the sample solution at the excitation wavelength, the necessary modification would be restricted to a minor addition to the differential amplifier circuit. Thus, the light intensity measurements at P_1 could be used to normalize the transmission value obtained at the exit of the amplifier *2 via* a variable gain amplifier.

Quantum yield measurements of strongly fluorescent photochemical systems require that the sample solutions are fully absorbing the incident light. In addition, recording of light emission by photoelement P_2 has to be avoided, *e.g.* by setting potentiometer *1* to zero.

Control Measurements and Calibration

The linearity of the reading of light transmission at 366 nm was checked using ethanolic solutions of MICHLER ketone of various concentrations. For this

[4] R.R. BIRGE and D.C. JOHNSON, *Rev. Sci. Instrum. 41* (1971) 1231.
[5] J. YGUERABIDE, *Rev. Sci. Instrum. 39* (1968) 1048.
[6] W.H. MELHUISH, *J. Opt. Soc. Amer. 52* (1962) 1256, *54* (1964) 183; *J. Physic. Chem. 65* (1961) 229.
[7] We thank Professor H. LABHART and Dr. W. HEINZELMANN for discussions and informations concerning their apparatus.
[8] *Cf.* W. SLAVIN, R.W. MOONEY and D.T. PALUMBO, *J. Opt. Soc. Amer. 51* (1961) 93, for the wavelength dependence of reflection from polished quartz surfaces.
[9] F. ECKOLDT and R. GEBHARDT, Telefunken-Applikationsbericht *Optoelektrische Bauelemente* (1970).
[10] The values of the resistor network were chosen to insure linearity in response for light fluxes of *ca.* $0.2 \cdot 10^{-6}$ to $1 \cdot 10^{-4}$ Einstein/min, appropriate for the emission intensity above 230 nm of the light source normally used in our system (a Hanovia 1000 W HgXe lamp with a single grating monochromator).
[11] The following consideration confirms that the integrated voltage is proportional to the number of quanta absorbed:

$$V_2 = \beta \cdot P(1-R)\, T \cdot I_0$$
$$V_1 = \beta \cdot R \cdot I_0$$
$$V_3 = K(V_1 - V_2) = K \cdot \beta [R \cdot I_0 - P(1-R)\, T \cdot I_0]$$

For $T = 1 \therefore V_3 = 0$ (balance condition),
consequently $P(1-R) = R$
and $V_3 = K \cdot \beta \cdot R(1-T)\, I_0$.

$V_{1,2}$ = Voltages at $P_{1,2}$, V_3 = voltage at entrance of *4*, β = proportionality factor for light conversion to V_1 and V_2, P = proportionality factor introduced by *1*, R = fraction of light reflected from *B*, T = transmission, I_0 = incident light intensity, K = proportionality factor given by gain of *2* and setting of *3*; *cf.* Fig. 3.

Table 1. Comparison of Quantum Yield Measurements with Literature Data [a]

Starting material	Products	Solvent	Φ 313 nm This work	Literature value
2-Phenyl-2-methylpropionaldehyde	Isopropyl benzene + CO	Iso-octane	0.83 [b]	0.76 ± 0.02 [13]
Valerophenone	Acetophenone + propene	Benzene	0.35 [c]	0.33 [14]
	1-Phenyl-2-methylcyclobutan-1-ols	*t*-Butyl alcohol	0.89 [c]	1.0 [14]
		t-Butyl alcohol	0.09 [c]	
		Benzene	0.06 [c]	0.07 [14]

[a] Sample solutions degassed by 4–6 freeze-pump(10^{-5} Torr)-thaw cycles; irradiation at 313 nm and 25° to 10–15% conversion; analyses by vapor phase chromatography.
[b] Quantum yield of decrease in starting material. This reaction is very sensitive to the presence of dissolved molecular oxygen.
[c] Quantum yield of product formation.

purpose, a digital voltmeter was connected to the differential amplifier *(2)*, and the ratio U_c/U_∞ (U_c = voltage at concentration c, U_∞ = voltage at infinite concentration, *i.e.*, at 0% transmission) was plotted against the transmissions measured spectrophotometrically at the same wavelength. A linear plot of unity slope was obtained within ± 1% over the full range of transmission, thus confirming a satisfactory correction of the integration at incomplete light absorption in the sample solution.

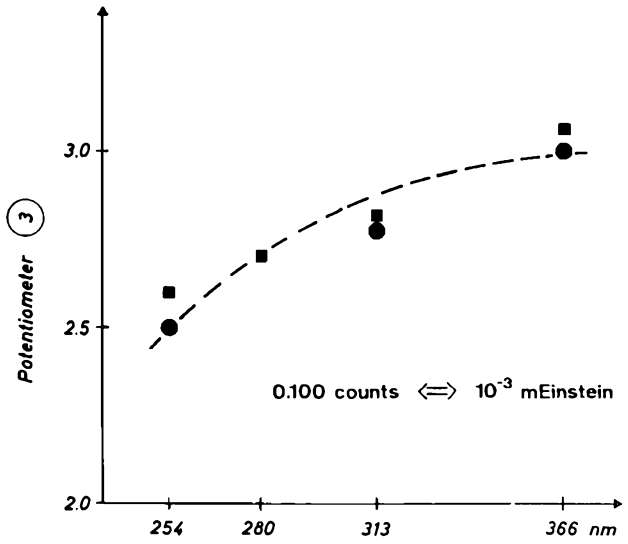

Fig. 4. Results of calibration with ferrioxalate actinometer (●, ■) matched against the curve obtained from calculated values for reflection at the quartz plate (---, inverse percentage of total light intensity arbitrarily fitted to coincide with one experimental calibration value at 366 nm)

Ferrioxalate actinometry[12] at wavelengths 254, 280, 313, and 366 nm was used for calibration. The integrator sensitivity was adjusted with the potentiometer *3* in such a way as to obtain a simple relation between the counter reading and the amount of absorbed light quanta *(i.e.*, 0.100 counts equal 10^{-3} mEinstein). The experimental results are given in Fig. 4. They show an excellent agreement with the values calculated (normalized to 366 nm) for reflection at the quartz plate *(B)*[8]. Similarly satisfactory results were obtained with the uranyl oxalate actinometer.

As an additional control, the quantum yields of two examples taken from the literature, the photodecarbonylation of 2-phenyl-2-methylpropionaldehyde[13] and the type II fragmentation and cyclization of valerophenone[14], were remeasured; see Table 1.

Acknowledgements

Financial support for this work by the Fonds National Suisse de la Recherche Scientifique and by Firmenich S.A., Geneva, is gratefully acknowledged. We thank Professors H. Labhart, W. Simon, and U. Wild for critical reading of the manuscript, and Mr. Ch. Bullinger for technical assistance.

Walter Amrein, Jean Gloor, and Kurt Schaffner

Département de Chimie Organique, Université de Genève, 1211 Genève 4

[12] C. G. Hatchard and C. A. Parker, *Proc. Roy. Soc. A 235* (1956) 518.
[13] H. Küntzel, H. Wolf and K. Schaffner, *Helv. Chim. Acta 54* (1971) 868.
[14] P. J. Wagner and A. E. Kemppainen, *J. Amer. Chem. Soc. 94* (1972) 7495.

Dehydration of γ-FeOOH: Direct Observation of the Mechanism *

Summary

The dehydration of γ-FeOOH to γ-Fe_2O_3 has been investigated by thermoanalytical, electron microscopic and X-ray diffraction methods, using single crystals of suitably small size as a starting material, in order to maintain short diffusion paths. While kinetical data alone are not conclusive, the electron micrographs show unambiguously how the reaction proceeds in the crystals: Strings of perfectly oriented γ-Fe_2O_3 crystallites of about 70 Å diameter and disordered lithium site vacancies extend into the undecomposed matrix crystal which can be distinguished from decomposed parts by direct imaging of the (120) lattice planes of 3 Å spacing. An atomistic interpretation of this result is given.

* Received March 13, 1974.

1 Introduction

A comprehensive study of reactions involving solids should, in our opinion, include formal kinetics as well as morphological, textural and structural investigations. In order to exclude the influence of the surface, there is a tendency to use fairly large crystals. Under such conditions, however, diffusion paths are too long and will *eo ipso* influence the reaction mechanism. Such kinetic data, however good, will thus be of little help to decide between several possible mechanisms. FEITKNECHT[1] has pointed out that *small* single crystals will be the most suitable substrate to investigate solid state reactions. Only one reaction, however, has been studied along these lines, namely the oxidation of Fe_3O_4 to γ-Fe_2O_3[2,3].

We have studied a basically different reaction, i.e. the thermal decomposition 2 γ-FeOOH→ γ-Fe_2O_3 + H_2O. The relations between the two lattices involved are well known[4,5]. More recently GALLAGHER[6] has concluded from spectroscopic investigations that the γ-FeOOH lattice contains a considerable percentage of molecular water due to the peculiar arrangement of the OH...O bonds which yields, through a temperature dependent equilibrium, water molecules already at room temperature.

2 Experimental

γ-FeOOH was prepared by adding 0,15 L $FeCl_2$ 0,2 M to 0,1 L H_2O and 0,1 L NH_3/NH_4Cl buffer (pH 7,5), and introducing air at a rate of 0,5 L/min at 50 C in a waterbath. To maintain pH 6, NH_3 0,1 M was added dropwise from a buret (about 0,66 L altogether) while the pH was observed continuously with a glass electrode. After about 2 h the suspension proved free of Fe^{2+} (o-phenthroline test), i.e. the reaction was completed. The yellow-brown precipitate was isolated in a centrifuge, washed, and dried at 60 C. Its BET surface was about 14 m^2/g.

For X-ray diffraction a de Wolff-Guinier camera and FeK_α radiation were used. Reflection profiles from a Philips-Norelco goniometer served to calculate crystallite size and lattice disorder. Direct observation of the crystals was undertaken using a Siemens Elmiskop I, a Hitachi HU-11 A, and a Hitachi HU-12 A electron microscope.

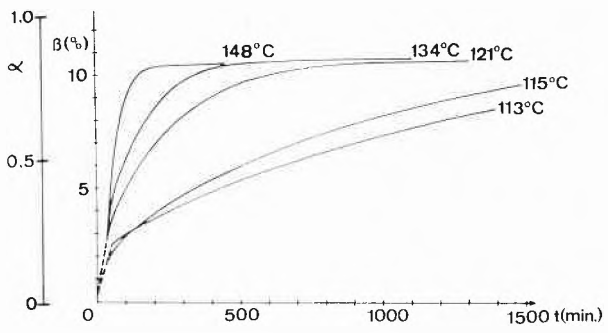

Fig. 1. Set of isothermal decomposition runs of γ-FeOOH. Abscissa: Time as measured, in minutes. Ordinates: β = weight loss in percent, before correction for adsorbed water. α = Reaction rate going from 0 to 1 (or 0 to 100%) without corrections

Unisothermal and isothermal decomposition was produced on a Mettler Thermoanalyzer TA 1 *in vacuo* (about 10^{-5} torr). Pt–Rh (10%) crucibles of 3, 12 and 16 mm diameter were used, with sample thickness not exceeding a few tenths of a mm. Evacuation and, under unisothermal conditions, heating rates, were as small as possible.

3 Results

Fig. 1 represents a typical set of decomposition curves under isothermal conditions. The reaction always ended sluggishly, and some residual water cannot be removed at all unless α-Fe_2O_3 nucleates.

When such results are plotted in a coordinate system with reduced time scale ($t/t_{½}$) on the abscissa and reaction rate 0 to 1 on the ordinate, fig. 2 results.

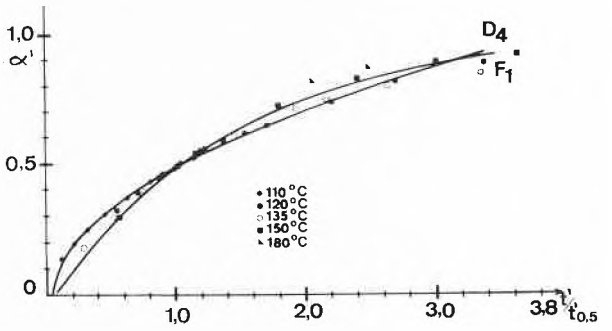

Fig. 2. Reduced time representation, after correction for adsorbed water, for isothermal decomposition of γ-FeOOH. The data used are a set different form that in fig. 1. Two calculated curves for different mechanism models from fig. 7 are also shown. α' = corrected reaction rate from 0 to 1 (or 0 to 100%)

The X-ray powder patterns of the samples undergoing decomposition (not shown here) are superpositions of the initial γ-FeOOH, with sharp reflections vanishing towards the end of the reaction, and of the γ-Fe_2O_3 pattern with extremely broad reflections. The profile analysis yields a crystallite size of the order of 70 Å and strong evidence for disorder, most probably in the vacant Lithium sites. It thus seems obvious that the tetragonal superlattice reflections of γ-Fe_2O_3 do not appear.

Electron micrographs of partly decomposed crystals show peculiar contrast phenomena which might be explained by strings of pores. As the crystals produce perfectly oriented electron diffraction textures (not shown here), these strings must be crystallites of γ-Fe_2O_3. Undecomposed crystals and, in partly decompo-

[1] W. FEITKNECHT, *Pure Appl. Chem. 9* (1964) 423.
[2] W. FEITKNECHT and U. MANNWEILER, *Helv. Chim. Acta 50* (1967) 570.
[3] K. J. GALLAGHER, W. FEITKNECHT and U. MANNWEILER, *Nature 217* (1968) 1118.
[4] J. D. BERNAL, D. R. DASGUPTA and A. L. MACKAY, *Nature 180* (1957) 645.
[5] D. R. DASGUPTA, *Ind. J. Physics 35* (1961) 401, and: T. TAKADA, M. KIYAMA and S. SHIMIZU, *Bull. Inst. Chem. Res. Kyoto Univ. 42* (1964) 505.
[6] K. J. GALLAGHER and D. N. PHILLIPS, unpublished.

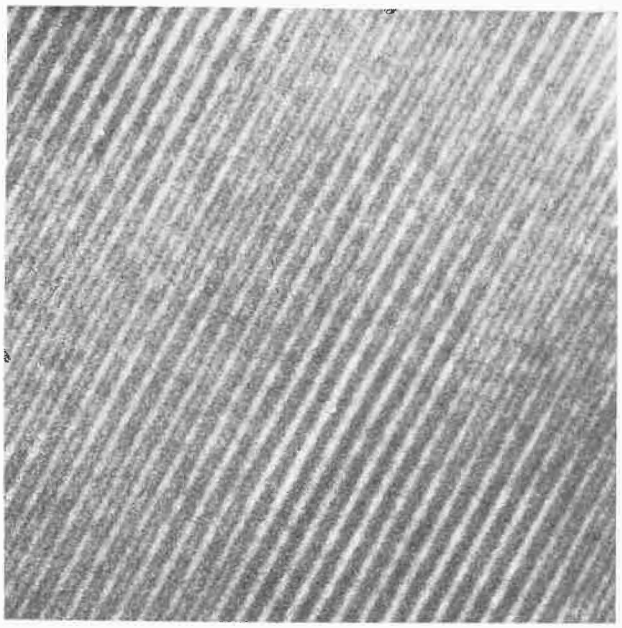

Fig. 3. Electron micrograph of undecomposed γ-FeOOH showing (120) lattice planes of spacing 3,3 Å. Hitachi HU-12A. Magnification 5 000 000

sed platelets, the undecomposed regions, exhibit the usual extinction contours (Bragg fringes) which show that this part of the lattice is scattering coherently*. In a few cases it was possible to make directly visible the (120) lattice planes of γ-FeOOH in undecomposed crystals (fig. 3).

4 Discussion and conclusions

The kinetical data (fig. 2) fit equally well into quite different functions as shown in the representation of SHARP *et al.*[8] (Fig. 5). An unambiguous answer from these results alone, hence, is impossible.

The additional evidence from electron micrographs, X-ray diffraction, electron diffraction and BET surface measurements, however, suggests the following mechanism.

In order to form the γ-Fe_2O_3 lattice, the corrugated layers of edge and corner sharing (FeO_6) octahedra of γ-FeOOH must collapse in the manner shown schematically in fig. 6. By the introduction of more edge and corner sharing, O^{2-} ions in the form of water are set free. The considerable lattice strain visualized in fig. 6 accompanied by additional shear in the two other directions of the lattice leads to the total disruption of the dehydrated region of γ-FeOOH. The front of such a region being under strain is a suitable nucleus for further reaction; the process thus continues along the needle axis *c*, starting usually from cracks or other defects at the edge of the crystal. The strings of 70 Å large γ-Fe_2O_3 crystallites produce the mentioned contrast phenomenon since their neighbourhood has to support

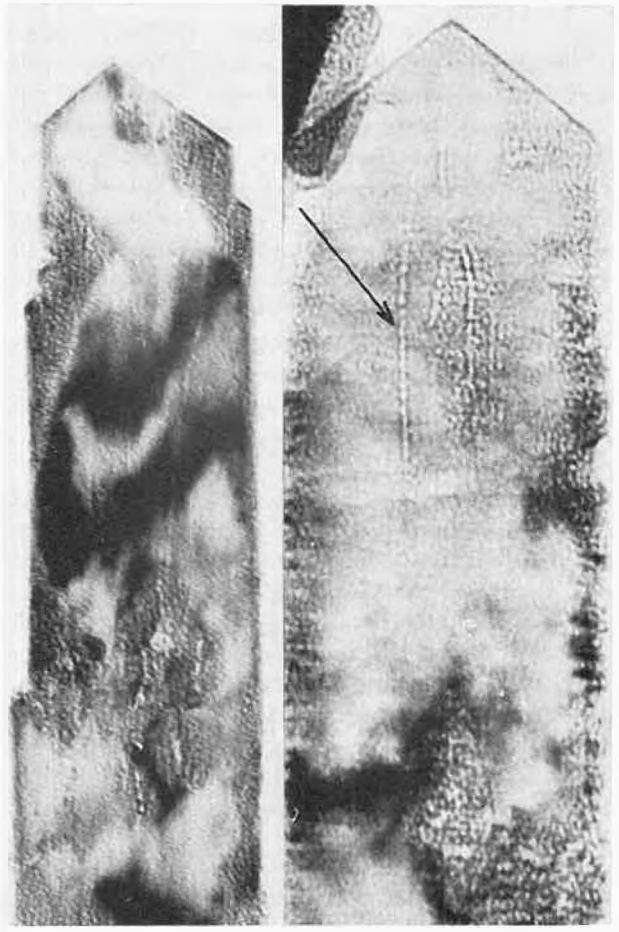

Fig. 4 Electron micrographs of partly decomposed γ-FeOOH crystals. Uniform grey regions with black extinction contours (Bragg fringes) are unaltered; other regions indicate complete dehydration. Instead of a sharp phase boundary, pearl-like strings intrude from decomposed regions into regions of unaltered γ-FeOOH. The visible crystallite size is consistent with 70 Å found from X-ray reflection profiles. BET measurements of the specific surface show that these features are not pores; hence they are crystallites of γ-Fe_2O_3 producing a considerable strain on the surrounding matrix, thus giving the contrast phenomenon. Arrow indicates strings of γ-Fe_2O_3. Magnification 200 000

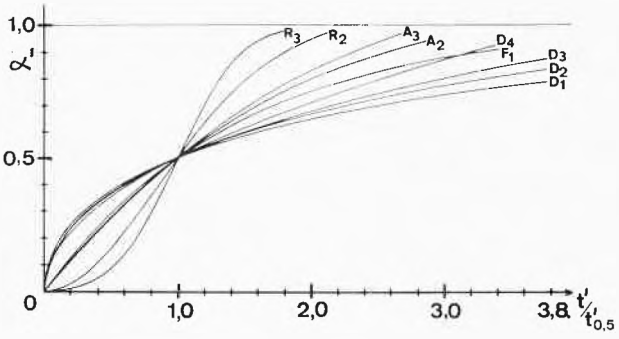

Fig. 5. Calculated rate curves representing various models of reaction mechanisms, after SHARP *et al.*[8] Reduced time scale and ordinate as fig. 2. *F* 1 = First order law (Random nucleation), *D* 1 to 4 = diffusion controlled mechanisms, *A* = Avrami equations, *R* = boundary controlled mechanism. For full explanation see reference [8]

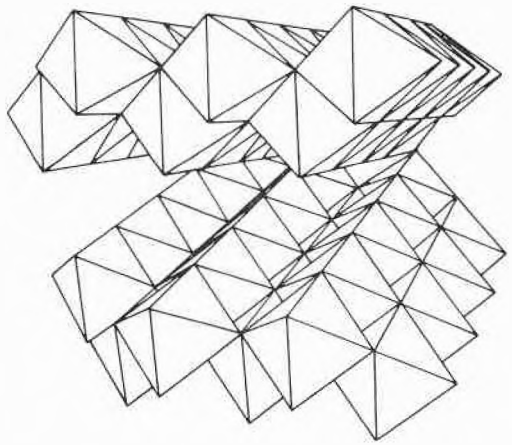

Fig. 6. Schematic three-dimensional representation of interface between undecomposed γ-FeOOH and final γ-Fe_2O_3, producing the considerable strain in the γ-FeOOH crystal and the contrast effect in the electron micrograph. The front of the picture represents the boehmite type lattice of γ-FeOOH (hydrogen bonds holding together the corrugated layers are omitted). Towards the background these layers approach each other until they collapse (in the back end of the figure).

From there the octahedra would extend further backwards forming essentially a cubic dense packing, i. e. the γ-Fe_2O_3 lattice. This representation showing the transition between the two lattices makes evident the total disruption of the initial crystal into numberless microcrystallites consisting of only about 5 to 10 unit cells. It also makes evident that in these microcrystals ordering to the perfect γ-Fe_2O_3 structure is not possible.

considerable shear and other strain. The contrast is best visible in the early stage of the dehydration, when it shows particularly well against the Bragg fringes uf the surrounding undecomposed matrix.

The final product has still a crystallite size of 70 Å. The residual water is therefore chemisorbed and cannot take off even *in vacuo*, hence the sluggish end part of the reaction. This might lead to the erroneous conclusion that γ-Fe_2O_3 is stable only in the presence of protons. FEITKNECHT[1,2] and GALLAGHER[3] have, however, shown that this view is incorrect.

The small crystallite size and the low temperature seem to suppress the rearrangement of the lattice disorder, as opposed to the ordering observed in γ-Fe_2O_3 cubes of about 30 times larger size in O_2 atmosphere.

A full account on this subject will be submitted to *Thermochimica Acta*.

We thank Professor W. FEITKNECHT and Dr. K. J. GALLAGHER for helpful discussions, Dr. H.-G. WIEDEMANN (Mettler Ltd). for permission to use apparatus and for other support, Mr. T. KAMINO for help to obtain lattice resolution, Miss ETTINGER for photographic work, and the Swiss National Fund for financial support.

RUDOLF GIOVANOLI und RUDOLF BRÜTSCH

Laboratory of Electron Microscopy
Institute of Inorganic Chemistry
University of Berne
Freiestrasse 3
P.O.B. 140, CH-3000 Berne 9 (Switzerland)

* Bragg fringes are bands in which the Bragg condition for diffraction is fulfilled and where coherently scattered parts of the electron beam are caught at the contrast aperture. Such "extinction contours" are therefore dark[7].

[7] L. REIMER, *Elektronenmikroskopische Untersuchungs- und Präparationsmethoden*, 2nd Edition, Springer, Berlin 1967, p. 191 ff.

[8] J. H. SHARP, G. W. BRINDLEY and B. N. NARAHARI ACHAR, *J. Amer. Ceram. Soc. 49* (1966) 379.